Vortex knots in a Bose-Einstein condensate

Davide Proment,[1,2,*] Miguel Onorato,[1,2] and Carlo F. Barenghi[3]
[1]*Dipartimento di Fisica, Università degli Studi di Torino, Via Pietro Giuria 1, 10125 Torino, Italy, EU*
[2]*INFN, Sezione di Torino, Via Pietro Giuria 1, 10125 Torino, Italy, EU*
[3]*School of Mathematics and Statistics, Newcastle University, Newcastle upon Tyne, NE1 7RU, United Kingdom, EU*
(Received 26 October 2011; published 19 March 2012)

We present a method for numerically building a vortex knot state in the superfluid wave function of a Bose-Einstein condensate. We integrate in time the governing Gross-Pitaevskii equation to determine evolution and shape preservation of the two (topologically) simplest vortex knots which can be wrapped over a torus. We find that the velocity of a vortex knot depends on the ratio of poloidal and toroidal radius: for smaller ratio, the knot travels faster. Finally, we show how vortex knots break up into vortex rings.

DOI: 10.1103/PhysRevE.85.036306 PACS number(s): 47.32.C−, 03.75.Lm

I. INTRODUCTION

In 1867, following the works of Helmholtz on vortices and of Riemann on Abelian functions, Lord Kelvin modeled atoms as knotted vortex tubes in ether [1], effectively giving birth to knot theory [2]. This discipline has fascinated mathematicians and physicists since. More recently, knots have been the studied in different branches of physics, ranging from classical fluid dynamics [3,4], magneto-hydrodynamics [5], and classical field theory [6], to superconductors [7,8], excitable media [9], optics [10,11], and liquid-crystal colloids [12].

Knots in superfluids are identified with closed vortex lines, regions of fluid around which the circulation assumes nonzero (quantized) value. Vortex rings have been studied experimentally in superfluid liquid helium [13,14] and in Bose-Einstein condensates [15]. Numerical simulations have revealed that superfluid turbulence contains linked vortex lines [16], but, to the best of our knowledge, individual vortices with nontrivial topology have never been observed directly. To shed light on this problem, energy, motion, and stability of vortex knots have been examined theoretically and numerically using the classical theory of thin-cored vortex filaments. In this approach, the governing incompressible Euler dynamics is expressed by the Biot-Savart law or by its local induction approximation (LIA). Considering the LIA limit, it has been conjectured [17] and recently proved [18,19] that any closed curve more (topologically) complex than a ring is linearly unstable to perturbation or changes its knot type during the evolution. However, when the full Biot-Savart model is considered, a stabilization effect is observed and, under certain conditions, it is found that some vortex knots travel and preserve the knot type without breaking up for distances larger than their own diameters [20,21].

In superfluid helium, the validity of the classical theory of thin-core vortex filaments is based on the large separation of scales between the vortex core radius a_0 (approximately 10^{-8} cm in ^{4}He and 10^{-6} cm in ^{3}He-B) and the typical distance ℓ between vortices. In turbulence experiments, $\ell \approx 10^{-3}$ to 10^{-4} cm; the last value is also the typical diameter of experimental vortex rings [14]. The situation is very different in atomic Bose-Einstein condensates, where ℓ is only few times larger than a_0. In this context, the Gross-Pitaevskii equation (GPE) is clearly a more realistic model [22], particularly at very low temperatures, as thermal effects can be neglected.

The advantage of the GPE is that it does not need the cut-off parameter required by the classical vortex filament theory to de-singularize the Biot-Savart integral [23]. The second advantage is that the GPE naturally describes vortex reconnections [24], which must be implemented algorithmically in the Biot-Savart model. Any prediction about the evolution, the shape preservation, and the breakup of a vortex structure which is not orders of magnitude bigger than a_0 is therefore more reliable if obtained using the GPE. The third advantage of searching for vortex knots in a Bose-Einstein condensate is that direct images of individual vortex structures are possible without the use of tracer particles which will certainly disturb these structures. The disadvantage is that atomic condensates are small, and thus the motion of these structures will be affected by the boundaries and by the nonuniformity density of the background condensate. Before investigating these effects, however, it is essential to establish whether vortex knot solutions of the governing GPE exist, and, if they do, if they are sufficiently long-lived structures. This is the limited aim which we set in this work.

We stress that we do not intend to propose a mechanism to experimentally create vortex knots in condensates, but only to study the possible existence and preservation of knot type of these solutions of the GPE. We shall see that even setting up a topologically nontrivial structure in the wave function numerically is not a minor task; indeed, to the best of our knowledge, this is the first time it has been done for a single scalar field describing the condensate order parameter. For completeness, we emphasize that the existence and stability of vortex knots in more complicated Bose systems have already been discussed using the Faddeev-Skyrme model [25–27], as in the case of a charged two-condensate Bose system [28], an interacting mixture of charged and neutral superfluid [29], and spinor condensates [30,31]. Related work on vortex unknots, notably, vortex rings perturbed by Kelvin waves, was carried out recently by Helm *et al.* [32] and Sonin [33].

The manuscript is organized as follows. Section II explains how to create an elementary vortex knot in the initial conditions of the condensate wave function. Section III deals with the analysis of the dynamical properties of vortex knots.

*davideproment@gmail.com; www.to.infn.it/∼proment

Section IV describes the breakup of vortex knots. Finally, the conclusions are in Sec. V.

II. VORTEX KNOT INITIAL CONDITIONS

We consider the defocusing GPE written in the following dimensionless form:

$$2i\,\partial_t\psi + \nabla^2\psi - |\psi|^2\psi = 0, \tag{1}$$

where no external confining potential is present. The characteristic length scale of perturbations of the uniform condensate, called *healing length*, is defined as

$$\xi = \frac{1}{\sqrt{\langle\rho\rangle}}, \text{ where } \langle\rho\rangle = \frac{1}{V}\int_V |\psi|^2 dV \tag{2}$$

is the mean density of the condensate. Besides the energy, the GPE conserves the total number of particles, and therefore ξ is a conserved quantity too. Without loss of generality, we choose to deal with a system that has an unperturbed density (the density field at infinity) equal to unity and assume that perturbations are localized in a small region of the sample. In this hypothesis, $\xi \simeq 1$ in our units.

We now explain how to numerically build a vortex knot. First we construct a vortex. Consider the two-dimensional plane sOz, that is to say, defined by the axes s and z lying on it. A stable vortex is a hole (zero value) in the density field around which the phase of the wave function changes by $\pm 2\pi$. A sufficiently accurate description of a two-dimensional vortex centered in the origin of the sOz plane is given by the wave function $\Psi_{2D}(s,z) = \sqrt{\rho(R)}\,e^{-i\,\theta(s,z)}$, where $R = \sqrt{s^2+z^2}$:

$$\begin{aligned}\rho(R) &= \frac{R^2(a_1 + a_2R^2)}{1 + b_1R^2 + b_2R^4},\\ \theta(s,z) &= \text{atan2}(z,s),\end{aligned} \tag{3}$$

atan2(...) being the extension of the arctangent function whose principal value is in the range $(-\pi;\pi]$, and the coefficients $a_1 = 11/32, a_2 = 11/384, b_1 = 1/3$, and $b_2 = 11/384$ arising from a second-order Padé approximation [34]. Figure 1 shows how the density field behaves around the axisymmetric vortex center.

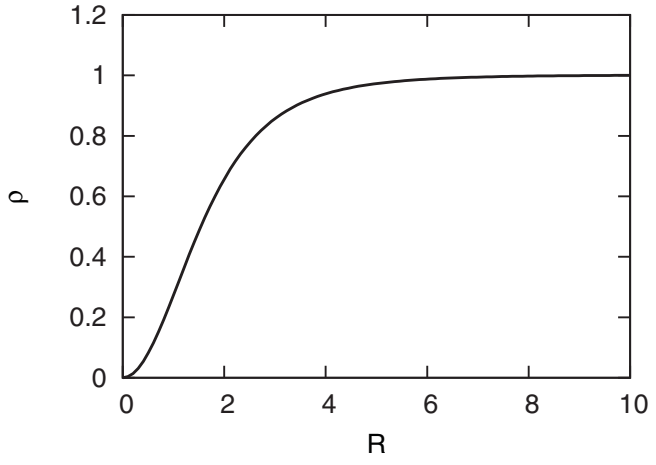

FIG. 1. The density field ρ around an axisymmetric two-dimensional vortex. Radial distances R are in units of the healing length ξ.

It is clear from the plot that the vortex core is of the order of the healing length, and the bulk value of the density $\rho = 1$ is recovered at larger distances.

We now come back to vortex knots in a three-dimensional system. We define a knot as a closed curve over a torus, characterized by the toroidal radius R_0 and the poloidal radius R_1. More precisely, a closed curve $\mathcal{T}_{p,q}$ on the torus is determined by counting the number of toroidal wraps p and the number of poloidal wraps q. For example, the curves $\mathcal{T}_{1,1}$ and $\mathcal{T}_{2,2}$ describe, respectively, the unknot (the simple vortex ring) and two unlinked rings. The first topologically nontrivial curve is the trefoil $\mathcal{T}_{2,3}$. In this work we shall focus on the two simplest knots, the trefoil $\mathcal{T}_{2,3}$ and its dual $\mathcal{T}_{3,2}$.

A. The $\mathcal{T}_{2,3}$ knot (trefoil)

The vortex line of a $\mathcal{T}_{2,3}$ knot lays on the torus as shown in Fig. 2. Any plane sOz passing through the z axis intercepts the curve $\mathcal{T}_{2,3}$ at four different points, which correspond to four two-dimensional point vortices on the plane sOz. The positions of these two-dimensional vortices vary with respect to the choice of the plane sOz; in other words, these positions are functions of the angle variable ϕ introduced in Fig. 2. For example, the vortex positions of the wave function for the angle $\phi = 0$ are shown in Fig. 3. By construction, these point vortices are located on the circumference defined by the intersection of the plane with the torus, and rotate on it following a particular function $f(\phi)$. To assure continuity of the vortex line and to describe the trefoil knot, the function $f(\phi)$ must have the form $f(\phi) = 3\phi/2$, with $\phi \in [0,\pi)$.

We are now ready to write the three-dimensional wave function which describes the trefoil knot $\mathcal{T}_{2,3}$. In the approximation that the healing length ξ is much smaller than the inter-vortex distance, the two-dimensional wave function in the plane sOz is given by the superposition (multiplication) of the wave function Ψ_{2D} of each two-dimensional vortex centered in the correct position, where the opposite circulation is obtained by

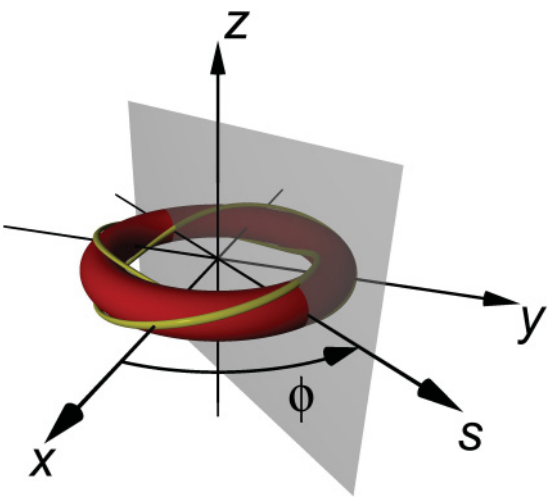

FIG. 2. (Color online) Construction of the trefoil knot $\mathcal{T}_{2,3}$.

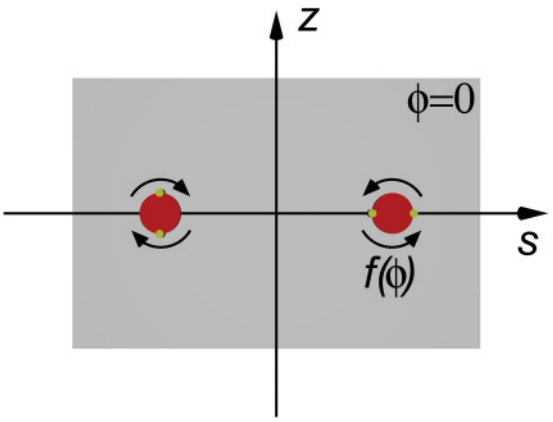

FIG. 3. (Color online) Positions of the four vortices on $\phi = 0$ used to construct the wave function of the trefoil knot $\mathcal{T}_{2,3}$. Clockwise and anticlockwise arrows describe the motion of vortex positions with respect to the function $f(\phi) = 3\phi/2$.

applying the complex conjugation operator $(...)^*$. Thus, the three-dimensional wave function results in

$$\begin{aligned}
&\psi_{2,3}(x,y,z)\\
&\quad = \Psi_{2D}\{s(x,y) - R_0 - R_1\cos[\alpha(x,y)], z - R_1\sin[\alpha(x,y)]\}\\
&\qquad \times \Psi_{2D}\{s(x,y) - R_0 - R_1\cos[\alpha(x,y)+\pi],\\
&\qquad z - R_1\sin[\alpha(x,y)+\pi]\}\\
&\qquad \times \Psi^*_{2D}\{s(x,y) + R_0 + R_1\cos[\alpha(x,y)],\\
&\qquad z - R_1\sin[\alpha(x,y)]\}\\
&\qquad \times \Psi^*_{2D}\{s(x,y) + R_0 + R_1\cos[\alpha(x,y)+\pi],\\
&\qquad z - R_1\sin[\alpha(x,y)+\pi]\},
\end{aligned} \tag{4}$$

with $s(x,y) = \mathrm{sgn}(x)\sqrt{x^2+y^2}$, where sgn(...) is the sign function, and $\alpha(x,y) = 3/2\,\mathrm{atan2}(y,x)$.

B. The $\mathcal{T}_{3,2}$ knot

The technique used to define the wave function of the trefoil knot can be extended to any other knot built on a torus. The $\mathcal{T}_{3,2}$ knot can be represented on the torus as shown in Fig. 4. In this case the generic plane sOz intersects the knot in six

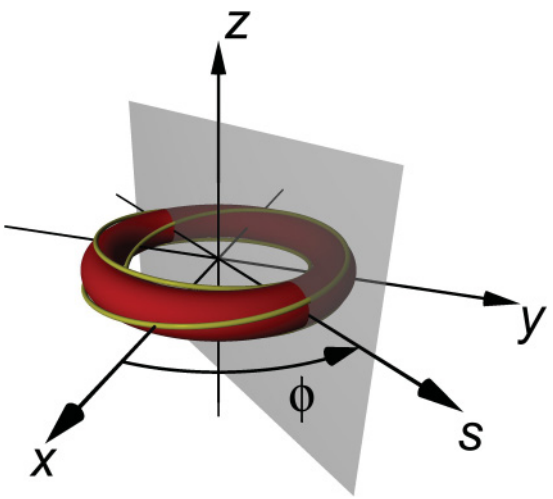

FIG. 4. (Color online) Construction of the trefoil knot $\mathcal{T}_{3,2}$.

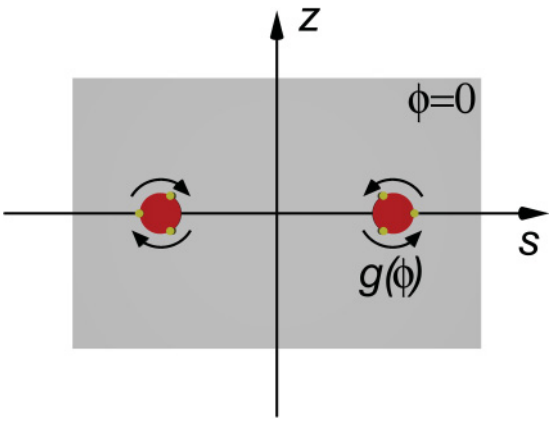

FIG. 5. (Color online) Positions of the six vortices on $\phi = 0$ used to construct the wave function of the knot $\mathcal{T}_{3,2}$. Clockwise and anticlockwise arrows describe the motion of vortex positions with respect to the function $g(\phi) = 2\phi/3$.

points, where the centers are a function $g(\phi)$ of the angle ϕ and rotate around the circumference defined by the plane and the torus intersection. An example of the configuration for $\phi = 0$ is shown in Fig. 5. The function $g(\phi)$ is $g(\phi) = 2\phi/3$, with $\phi \in [0,\pi)$.

Again, using the two-dimensional vortex description Ψ_{2D}, in the limit of intervortex distance much greater than the healing length ξ, the three-dimensional wave function of a $\mathcal{T}_{3,2}$ knot is

$$\begin{aligned}
&\psi_{3,2}(x,y,z)\\
&\quad = \Psi_{2D}\{s(x,y) - R_0 - R_1\cos[\alpha(x,y)], z - R_1\sin[\alpha(x,y)]\}\\
&\qquad \times \Psi_{2D}\{s(x,y) - R_0 - R_1\cos[\alpha(x,y)+2\pi/3],\\
&\qquad z - R_1\sin[\alpha(x,y)+2\pi/3]\}\\
&\qquad \times \Psi_{2D}\{s(x,y) - R_0 - R_1\cos[\alpha(x,y)+4\pi/3],\\
&\qquad z - R_1\sin[\alpha(x,y)+4\pi/3]\}\\
&\qquad \times \Psi^*_{2D}\{s(x,y) + R_0 + R_1\cos[\alpha(x,y)],\\
&\qquad z - R_1\sin[\alpha(x,y)]\}\\
&\qquad \times \Psi^*_{2D}\{s(x,y) + R_0 + R_1\cos[\alpha(x,y)+2\pi/3],
\end{aligned}$$

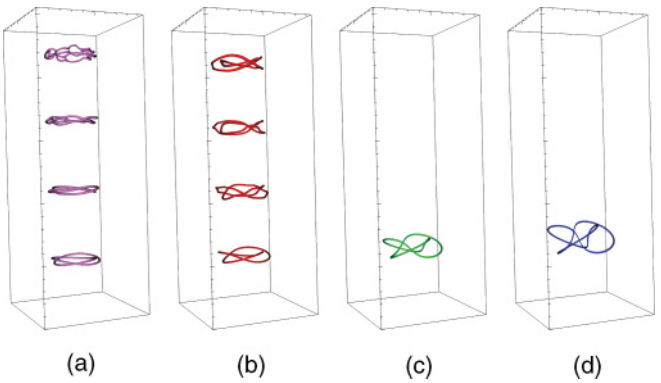

FIG. 6. (Color online) Isosurfaces of the density field at the threshold level $\rho_{\mathrm{th}} = 0.2$ for $\mathcal{T}_{2,3}$ knots of various knot ratios R_1/R_0 (see Table I). Snapshots at times $t = 0,400,800,1200$. Unstable knots are not shown. For complete evolution movies refer to [37].

TABLE I. Vortex knot parameters of $\mathcal{T}_{2,3}$ and $\mathcal{T}_{3,2}$ used in the simulations.

Case $\mathcal{T}_{2,3}$–$\mathcal{T}_{3,2}$	Knot ratio R_1/R_0	Max size $2(R_0+R_1)$	Min size $2R_1$	Break up Yes/No
(a)–(a)	1/10	44ξ	4ξ	N–N
(b)–(b)	1/5	48ξ	8ξ	N–N
(c)–(c)	2/5	56ξ	16ξ	Y–Y
(d)–(d)	3/5	64ξ	24ξ	Y–Y

$$z - R_1 \sin[\alpha(x,y) + 2\pi/3]\}$$
$$\times \Psi^*_{2D}\{s(x,y) + R_0 + R_1 \cos[\alpha(x,y) + 4\pi/3],$$
$$z - R_1 \sin[\alpha(x,y) + 4\pi/3]\}, \quad (5)$$

with $s(x,y) = \mathrm{sgn}(x)\sqrt{x^2+y^2}$ and $\alpha(x,y) = 2/3\,\mathrm{atan2}(y,x)$.

III. VORTEX KNOT DYNAMICS

To study the dynamics and shape preservation of the knots $\mathcal{T}_{2,3}$ and $\mathcal{T}_{3,2}$ with different geometries, we have to find a compromise between the accessible numerical resolution and the box size: we need to resolve small scales near the vortex cores and, at the same time, minimize the finite size (boundary) effects. We recall that the parameters which identify our vortex knots, the toroidal and poloidal radii R_0 and R_1, are expressed in units of the healing length ξ.

We chose to uniformly discretize physical space using a Cartesian grid with steps $\Delta x = \Delta y = \Delta z = 0.5\,\xi$ spanning over the *knot ratios* $R_1/R_0 = 1/10, 1/5, 2/5, 3/5$. We expect vortex knots to behave similarly to vortex rings, that is to say, we expect that they travel along the direction of the torus axis of symmetry (the z axis). Taking our computational constraints into account, we use $192 \times 192 \times 512$ grid points ($L_x = L_y = 96\,\xi$ and $L_z = 256\,\xi$) and the toroidal radius $R_0 = 20\,\xi$. This choice allows us to have a minimum value of $R_1 = 2\,\xi$ (when $R_1/R_0 = 1/10$), acceptable to observe the small intervortex interactions, and a maximum knot size of $2(R_0+R_1) = 64\,\xi$ (when $R_1/R_0 = 3/5$), which gives tolerable boundary effects. Table I summarizes the simulation parameters.

In order to let the knot travel for the maximum distance in the z direction, at the start of the calculation ($t = 0$) the vortex knot is centered at the point $[L_x/2, L_y/2, 2(R_0+R_1)]$. With this choice, the knot can propagate for a distance of 3 to $53/11 \simeq 4.8$ times its maximum size before hitting the opposite side of the computational domain corresponding to $z = L_z$. The GPE is integrated in time using a split-step method with antiperiodic (reflective) boundary conditions. The integration time step is $\Delta t = 0.02$ smaller that the fastest linear period $T_c \simeq 0.032$. This value allows us to conserve the initial energy and mass up to 3% and 1%, respectively, in all the simulations. Details on the numerical algorithm can be found in Refs. [35,36].

Figures 6 and 7 show the isosurfaces of the density field corresponding to the threshold value $\rho_{\mathrm{th}} = 0.2$ at the initial conditions and at successive times for the $\mathcal{T}_{2,3}$ and $\mathcal{T}_{3,2}$ knots, respectively (broken knots will be discussed in the next section). As expected, vortex knots move along the z direction (the axis of symmetry of the torus), but also twist around it. Qualitatively, vortex knots with small knot ratio R_1/R_0 are fast and long-lived, as they propagate along the z direction

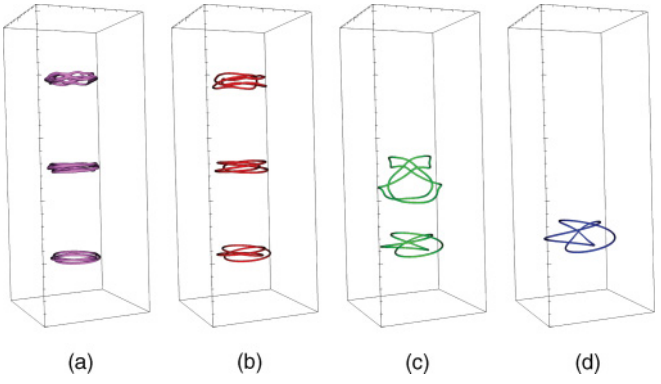

FIG. 7. (Color online) Isosurfaces of the density field at the threshold level $\rho_{\mathrm{th}} = 0.2$ for $\mathcal{T}_{3,2}$ knots of various knot ratios R_1/R_0 (see Table I). Snapshots at times to $t = 0, 400, 800$. Unstable knots are not shown. For complete evolution movies refer to [37].

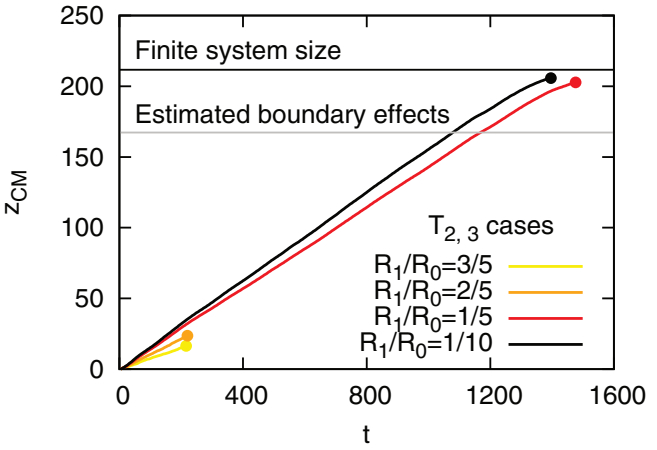

FIG. 8. (Color online) Position along the z axis (in units of the healing length) of the center of mass of $\mathcal{T}_{2,3}$ knots of various knot ratios R_1/R_0 as a function of time. The filled points denote the position where vortex knots break up. The horizontal lines denote, respectively, the distance where boundary effects become non-negligible and the finite system size along z.

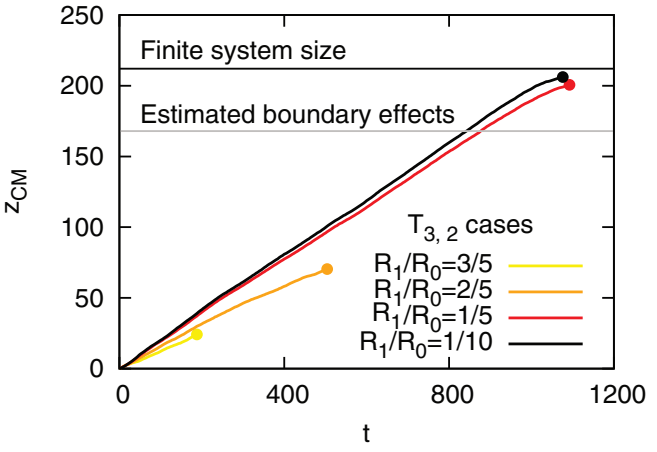

FIG. 9. (Color online) As in Fig. 8 but for $\mathcal{T}_{3,2}$.

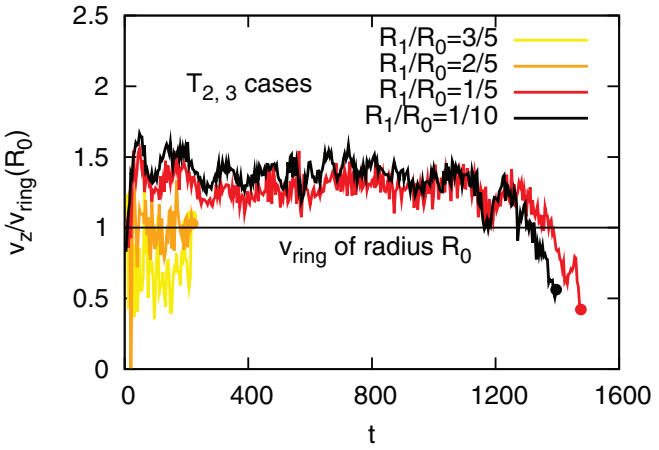

FIG. 10. (Color online) Velocity component v_z of $\mathcal{T}_{2,3}$ versus time of knots with various knot ratios R_1/R_0 before destroying (filled points). Velocities are expressed in units of vortex ring velocity (7) with quantum number $n = 1$ and radius $R = R_0$.

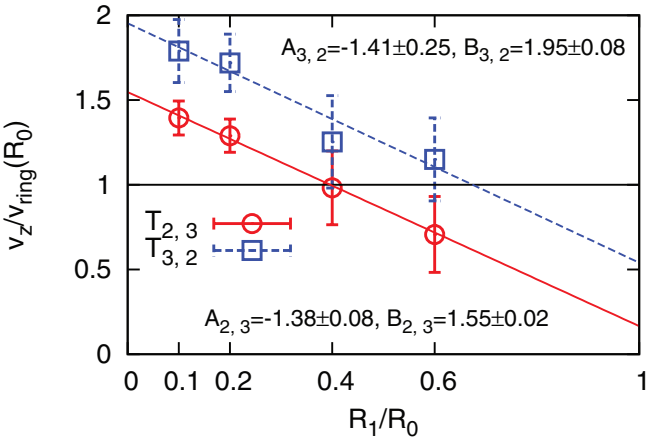

FIG. 12. (Color online) Averaged velocity components v_z of $\mathcal{T}_{2,3}$ and $\mathcal{T}_{3,2}$ vortex knots with various knot ratios R_1/R_0. Velocities are expressed in units of vortex ring velocity (7) with quantum number $n = 1$ and radius $R = R_0$. Error bars correspond to one standard deviation.

without breaking. During the evolution, Kelvin waves [13] appear; such waves are visible at the last stages of cases (a) and (b).

In order to quantify the evolution of vortex knots and compare one knot with others, we define the knot center of mass $\mathbf{r}_{CM} = (x_{CM}, y_{CM}, z_{CM})$ as

$$\mathbf{r}_{CM} = \frac{\int_V \mathbf{r}\, H(\rho_{\rm th} - |\psi|^2)\, dV}{\int_V H(\rho_{\rm th} - |\psi|^2) dV}, \tag{6}$$

where $H(...)$ is the Heaviside step function. Figures 8 and 9 show the z component z_{CM} of the knot center of mass (shifted with respect to the initial position) for the $\mathcal{T}_{2,3}$ and $\mathcal{T}_{3,2}$ cases, respectively. In both cases, knots with smaller knot ratio R_1/R_0 move faster and propagate for longer distances before breaking up (a filled point at the end of each curve marks the breakup point).

The z component of the velocity of a vortex knot is estimated by evaluating $v_z(t) = [z_{CM}(t+\tau) - z_{CM}(t)]/\tau$ (where $\tau = 4$ for numerical convenience). Figures 10 and 11 show $v_z(t)$ measured in units of the vortex ring velocity [38]:

$$v_{\rm ring}(R) = \frac{n\kappa}{4\pi R}\left[\ln\left(\frac{8R}{\xi}\right) - 0.615\right], \tag{7}$$

having quantum number $n = 1$ and radius $R = R_0$ (note that in our nondimensional system the quantum of circulation is $\kappa = 2\pi$). It is apparent that vortex knots move with approximately constant z velocity before either breaking up or reaching the boundary of the computational domain, where the interaction with the image slows them down.

It is instructive to analyze the mean and the standard deviation of the vortex knots' velocities measured in the constant-velocity regimes. The results, expressed in units of $v_{\rm ring}(R_0)$, are shown in Fig. 12. Three conclusions can be drawn from this figure:

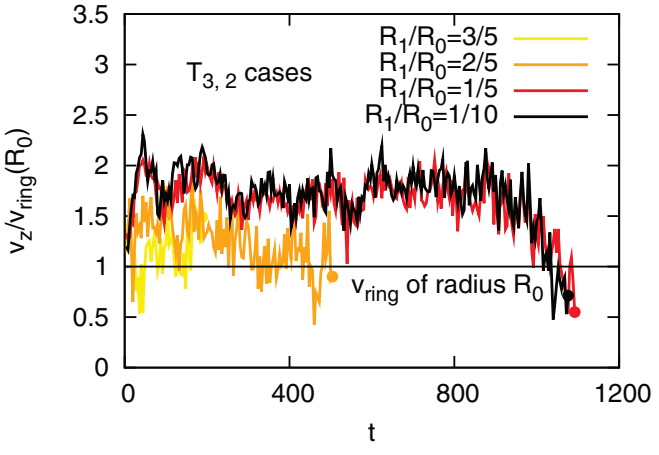

FIG. 11. (Color online) As in Fig. 10 but for $\mathcal{T}_{3,2}$.

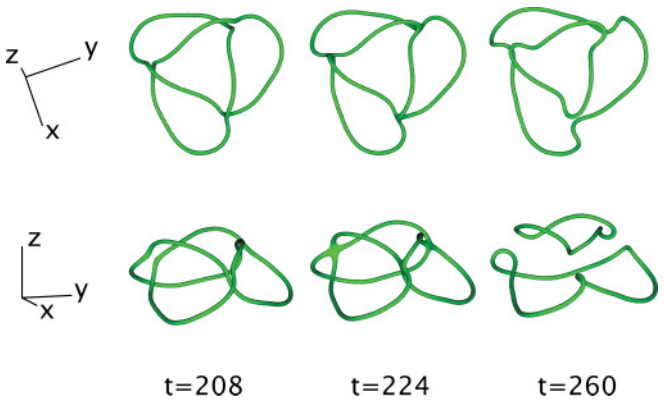

FIG. 13. (Color online) Three successive snapshots showing how the $\mathcal{T}_{2,3}$ vortex knot with knot ratio $R_1/R_0 = 2/5$ breaks up into two vortex rings. Here we plot two perspectives (up and to the side of the vortex propagation) of the isosurfaces of the density field corresponding to the threshold level $\rho_{\rm th} = 0.2$. For a complete evolution movie refer to [37].

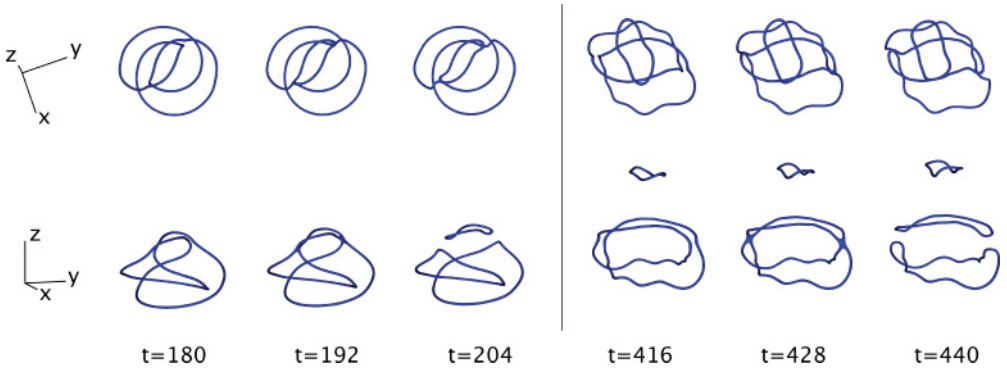

FIG. 14. (Color online) Two sequences of three successive snapshots showing how the $\mathcal{T}_{3,2}$ vortex knot with knot ratio $R_1/R_0 = 3/5$ breaks up into three vortex rings. Here we plot two perspectives (up and to the side of the vortex propagation) of the isosurfaces of the density field corresponding to the threshold level $\rho_{\rm th} = 0.2$. For a complete evolution movie refer to [37].

(1) $\mathcal{T}_{2,3}$ knots are slower than $\mathcal{T}_{3,2}$ knots with the same knot ratio. This is physically expected as the velocity field of torus knots at large distance is similar to the velocity field of vortex rings with multiple circulation: $\mathcal{T}_{2,3}$ corresponds to circulation of 2κ and $\mathcal{T}_{3,2}$ to 3κ. According to Eq. (7), the velocity is directly proportional to the circulation, and so $\mathcal{T}_{2,3}$ knots should be slower than $\mathcal{T}_{3,2}$ ones. However, this simple consideration does not apply well to knots, because we would have expected, for the small knot ratio tested ($R_1/R_0 = 1/10$), a scaled velocity of $v_z/v_{\rm ring}(R_0) \simeq 2$ and $v_z/v_{\rm ring}(R_0) \simeq 3$ for $\mathcal{T}_{2,3}$ and $\mathcal{T}_{3,2}$ respectively, and this is not the case.

(2) The z-velocity component scales with the knot ratio and can be parametrized as

$$v_z\left(\frac{R_1}{R_0}\right) = A_{p,q}\frac{R_1}{R_0} + B_{p,q}, \tag{8}$$

where $A_{p,q}$ and $B_{p,q}$ are coefficients which refer to the generic torus knot $\mathcal{T}_{p,q}$. Values of $A_{p,q}$ and $B_{p,q}$ for the knots $\mathcal{T}_{2,3}$ and $\mathcal{T}_{3,2}$ are reported in Fig. 12. It is interesting to observe that $A_{2,3} \simeq A_{3,2}$, indicating an evidence of universality for a generic knot which will be studied in future works.

(3) The z-velocity component of short-lived knots (i.e., knots that decay before reaching the computational boundaries) is less or similar to $v_{\rm ring}(R_0)$. On the contrary, knots that preserve their shapes within the computational domain are characterized by $v_z > v_{\rm ring}(R_0)$.

IV. THE BREAKING OF A KNOT

In our simulations we have observed that some vortex knots break up into topologically simpler objects [37]. We first analyze the unstable $\mathcal{T}_{2,3}$ knots; these are knots corresponding to knot ratios $R_1/R_0 = 2/5, 3/5$. In Fig. 13 we show three snapshots of the decay of the $\mathcal{T}_{2,3}$ knot with ratio $R_1/R_0 = 2/5$. It is apparent that the knot breaks into two vortex rings via three simultaneous self-reconnection events (see, in particular, the snapshot corresponding to $t = 224$). The decay of the vortex knot $\mathcal{T}_{2,3}$ with ratio $R_1/R_0 = 3/5$, not shown here, is similar.

On the contrary, $\mathcal{T}_{3,2}$ vortex knots break in a different manner. As shown in Fig. 14, the vortex knot $\mathcal{T}_{3,2}$ with knot ratio $R_1/R_0 = 3/5$ first decays in one vortex ring and two linked vortex rings via two simultaneous self-reconnection events (snapshot at time $t = 192$). Subsequently, the small free ring escapes from the other rings, which undergo two simultaneous reconnection events that create two unlinked vortex rings (snapshot at time $t = 428$). The last step is remarkable: there is no apparent reason why two linked vortex knots should in principle unlink into two vortex rings (by making two simultaneous reconnection events) without forming a single ring (by one reconnection event).

The $\mathcal{T}_{3,2}$ vortex knot with ratio $R_1/R_0 = 2/5$ qualitatively decays in the same way, producing a set of three unlinked vortex rings, but the steps are quite different. In the first step, a free vortex ring and two linked vortex rings are again produced. However, the free ring, which is initially located behind the two linked vortex rings, is smaller and faster than the other rings. As a consequence, it reconnects with the two linked vortex rings, as shown in Fig. 15 (snapshot $t = 752$). At this point the reformed knot breaks up, undergoing the same sequence previously described for the $\mathcal{T}_{3,2}$ with ratio $R_0/R_1 = 3/5$ case,

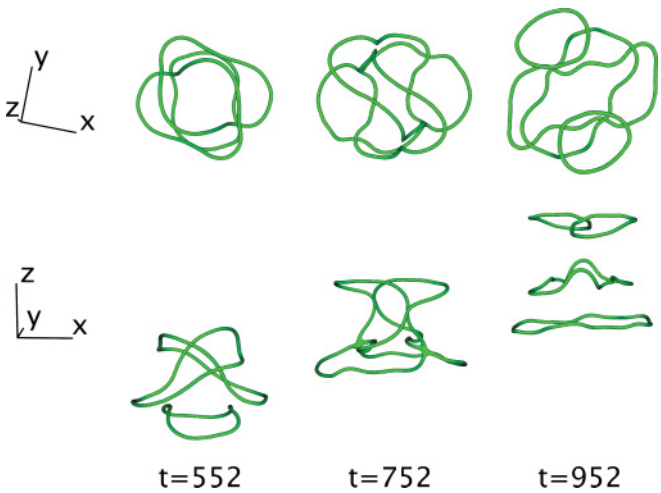

FIG. 15. (Color online) Three successive snapshots showing how the $\mathcal{T}_{3,2}$ knot with knot ratio $R_1/R_0 = 2/5$ breaks into three vortex rings. Here we plot two perspectives (up and to the side of the vortex propagation) of the isosurfaces of the density field corresponding to the threshold $\rho_{\rm th} = 0.2$. For a complete evolution movie refer to [37].

and the outcome is a set of three vortex rings (snapshot at time $t = 952$). Note that, in the last snapshot, the first knot (in the sense of the position) has split into two smaller vortex rings via a self-reconnection event which is probably a consequence of its Kelvin wave oscillations.

V. CONCLUSIONS

We have numerically analyzed the existence and evolution of vortex knots in the GPE model of a single scalar condensate. We have proposed a novel numerical technique for creating *ab initio* vortex knots in the wave function of the condensate. In particular, we have focused our numerical computations on the two simplest (in the topological sense) vortex knots, $\mathcal{T}_{2,3}$ and the $\mathcal{T}_{3,2}$.

We have analyzed the shape preservation of such knots with respect to the knot ratio R_1/R_0. We have found that a knot can break up into simple rings during the propagation, or preserve its knot type within our computational domain. Our numerical experiments clearly show that a small knot ratio ($R_1/R_0 = 1/10, 1/5$) increases the lifetime, whereas a large knot ratio ($R_1/R_0 = 2/5, 3/5$) decreases it, in agreement with [20]. In the LIA limit it is proved that any torus knots $\mathcal{T}_{p,q}$ with $p > q > 1$ are unstable, while in the case $q > p$ a knot could be neutrally stable but quickly changes its knot type during the evolution [18]. However, in our results using the Gross-Pitaevskii model, these differences do not seem to occur, as for small knot ratios both $\mathcal{T}_{2,3}$ and $\mathcal{T}_{3,2}$ behave similarly, are long-lived structures, and preserve their shape within our computational box.

We have found that vortex knots propagate essentially as vortex rings. We have measured the vortex knot velocities along the torus symmetry axis and shown that the velocity depends linearly on the knot ratio for both $\mathcal{T}_{2,3}$ and $\mathcal{T}_{3,2}$.

Finally, we have studied the details of the breakup of vortex knots. Although we do not have a theoretical explanation for the breakup, we have observed evidences of generic breaking behavior: $\mathcal{T}_{2,3}$ knots always break into two vortex rings via a three simultaneous self-reconnection event, whereas $\mathcal{T}_{2,3}$ knots first decay into three vortex rings via two simultaneous self-reconnections which create a free ring and two linked rings, then undergo two simultaneous reconnections which split the resulting link.

We believe that our work opens up new interesting problems in the field of fluid topology applied to superfluids and Bose-Einstein condensates. The natural developments of our study will be a theoretical investigation of the stability of vortex knots and an experimental study of the creation of a knotted initial condition in an atomic condensate.

ACKNOWLEDGMENTS

The authors acknowledge G. Boffetta, F. De Lillo, A. L. Fetter, and A. J. Youd for comments and suggestions, and a CINECA Award (No. HP10BQW4X9) 2011 for the availability of high-performance computing resources and support. C.F.B. is grateful to the Leverhulme Trust and to the EPSRC for financial support. D.P. expresses his gratitude to LLNS VISIT, POV-RAY, and GNUPLOT developers for the free software used for the visualization of numerical results.

[1] W. H. Thomson, Trans.-R. Soc. Edinburgh **25**, 217 (1869).
[2] C. Adams, *The Knot Book* (W.H. Freeman Publishers, New York, 1994).
[3] H. K. Moffatt, J. Fluid Mech. **35**, 117 (1969).
[4] H. K. Moffatt, Nature (London) **347**, 367 (1990).
[5] A. Y. K. Chui and H. K. Moffatt, Proc. Math. Phys. Sci. **451**, 609 (1995).
[6] L. Faddeev and A. J. Niemi, Nature (London) **387**, 58 (1997).
[7] E. Babaev, Phys. Rev. Lett. **88**, 177002 (2002).
[8] E. Babaev, Phys. Rev. B **79**, 104506 (2009).
[9] P. M. Sutcliffe and A. T. Winfree, Phys. Rev. E **68**, 016218 (2003).
[10] J. Leach, M. R. Dennis, J. Courtial, and M. J. Padgett, Nature (London) **432**, 165 (2004).
[11] M. R. Dennis, R. P. King, B. Jack, K. O'Holleran, and M. J. Padgett, Nat. Phys. **6**, 118 (2010).
[12] U. Tkalec, M. Ravnik, S. Copar, S. Zumer, and I. Musevic, Science **333**, 62 (2011), [http://www.sciencemag.org/content/333/6038/62.full.pdf].
[13] R. Donnelly, *Quantized Vortices in Helium II*, Vol. 3 (Cambridge University Press, Cambridge, UK, 1991).
[14] P. M. Walmsley and A. I. Golov, Phys. Rev. Lett. **100**, 245301 (2008).
[15] B. P. Anderson, P. C. Haljan, C. A. Regal, D. L. Feder, L. A. Collins, C. W. Clark, and E. A. Cornell, Phys. Rev. Lett. **86**, 2926 (2001).
[16] D. R. Poole, H. Scoffield, C. F. Barenghi, and D. C. Samuels, J. Low Temp. Phys. **132**, 97 (2003).
[17] S. Kida, J. Phys. Soc. Jpn. **51**, 1655 (1982).
[18] A. Calini and T. Ivey, J. Phys. A: Math. Theor. **44**, 335204 (2011).
[19] A. Calini, S. F. Keith, and S. Lafortune, Nonlinearity **24**, 3555 (2011).
[20] R. Ricca, D. C. Samuels, and C. F. Barenghi, J. Fluid Mech. **391**, 29 (1999).
[21] F. Maggioni, S. Alamri, C. F. Barenghi, and R. L. Ricca, Phys. Rev. E **82**, 026309 (2010).
[22] L. Pitaevskii and S. Stringari, *Bose-Einstein Condensation*, Vol. 116 (Oxford University Press, New York, 2003).
[23] P. G. Saffman, *Vortex Dynamics* (Cambridge University Press, Cambridge, UK, 1991).
[24] J. Koplik and H. Levine, Phys. Rev. Lett. **71**, 1375 (1993).
[25] J. Hietarinta, J. Jäykkä, and P. Salo, in proceedings of the Workshop on Integrable Theories, Solitons and Duality, PoS(unesp2002) (SISSA, Trieste, 2002), article ID 017.
[26] M. Kobayashi, J. Phys.: Conf. Ser. **297**, 012013 (2011).
[27] J. Hietarinta, J. Palmu, J. Jäykkä, and P. Pakkanen, New J. Phys. **14**, 013013 (2012).

[28] E. Babaev, L. D. Faddeev, and A. J. Niemi, Phys. Rev. B **65**, 100512 (2002).
[29] E. Babaev, Phys. Rev. D **70**, 043001 (2004).
[30] Y. Kawaguchi, M. Nitta, and M. Ueda, Phys. Rev. Lett. **100**, 180403 (2008).
[31] J. Liang, X. Liu, and Y. Duan, Europhys. Lett. **86**, 10008 (2009).
[32] J. L. Helm, C. F. Barenghi, and A. J. Youd, Phys. Rev. A **83**, 045601 (2011).
[33] E. B. Sonin, Europhys. Lett. **97**, 46002 (2012).
[34] N. Berloff, J. Phys. A: Math. Gen. **37**, 1617 (2004).
[35] D. Proment, S. Nazarenko, and M. Onorato, *Special Issue on Small Scale Turbulence*, Physica D: Nonlinear Phenom. **241**, 304 (2012).
[36] W. Bao and H. Wang, J. Comput. Phys. **217**, 612 (2006).
[37] See Supplemental Material at http://link.aps.org/supplemental/10.1103/PhysRevE.85.036306 for movies showing knot dynamics of five different simulations, including evolution of long-lived knots and breakup of short-lived knots.
[38] P. Roberts and J. Grant, J. Phys. A: Gen. Phys. **4**, 55 (1971).